Environmental Science and Pollution Research (2020) 27:5584–5594
https://doi.org/10.1007/s11356-019-07306-0

RESEARCH ARTICLE

Influence of *Leifsonia* sp. on U(VI) removal efficiency and the Fe–U precipitates by zero-valent iron

Shuibo Xie[1] · Xue Xiao[2] · Wenfa Tan[2,3] · Junwen Lv[2] · Qinwen Deng[3] · Qi Fang[2]

Received: 25 June 2019 / Accepted: 5 December 2019 / Published online: 18 December 2019

Abstract

Zero-valent iron (ZVI) has been widely applied to the remediation of uranium (U)-contaminated water. Notably, indigenous bacteria may possess potential positive or unfavorable influence on the mechanism and stability of Fe–U precipitates. However, the focus of the researches in this field has mainly been on physical and/or chemical aspects. In this study, batch experiments were conducted to explore the effects of an indigenous bacterium (*Leifsonia* sp.) on Fe–U precipitates and the corresponding removal efficiency by ZVI under different environmental factors. The results showed that the removal rate and capacity of U(VI) was significantly inhibited and decreased by ZVI when the pH increased to near-neutral level (pH = 6~8). However, in the ZVI + *Leifsonia* sp. coexistence system, the U(VI) removal efficiency were maintained at high levels (over 90%) within the experimental scope (pH = 3~8). This revealed that *Leifsonia* sp. had a synergistic effect on U(VI) remove by ZVI. According to scanning electron microscope and energy dispersive X-ray detector (SEM-EDX) analysis, dense scaly uranium-phosphate precipitation was observed on ZVI + *Leifsonia* sp. surface. The X-photoelectron spectroscopy (XPS) and Fourier transform infrared spectroscopy (FTIR) analysis indicated that *Leifsonia* sp. facilitated the generation of U(VI)-phosphates precipitates. The X-ray diffraction (XRD) analyses further revealed that new substances, such as $(Fe(II)Fe(III)_2(PO_4)_2(OH)_2)$, $Fe(II)(UO_2)_2(PO_4)_2 \cdot 8H_2O$, $Fe(II)Fe(III)_5(PO_4)_4(OH)_2 \cdot 4H_2O$, etc., were produced in the coexisting system of ZVI and *Leifsonia* sp. This study provides new insights on the feasibility and validity of site application of ZVI to U(VI)-contaminated subsurface water in situ.

Keywords Zero-valent iron · *Leifsonia* sp. · Uranium immobilization · Bacteria influence · Adsorption capacity · Precipitate

Introduction

Decades of nuclear-related activities such as U(VI) mining, nuclear weapon manufacturing, and nuclear fuel processing have produced a great amount of uranium-bearing waste rocks, uranium tailings, and uranium-bearing wastewater. Studies have reported that more than 4000 mines around the world generated a total estimated volume of 1 billion cubic meters of tailings (Černe et al. 2018; Mkandawire 2013). Long-term rainwater erosion and soil infiltration of the uranium tailing piles continuously cause the migration of U(VI), posing a great threat to the surrounding human health through the food chain (Basu et al. 2015; Liu et al. 2017; Soudek et al. 2010). Generally, the dominant states of U in groundwater/aquifer soil environment are mainly U(IV) and U(VI). U(IV) usually exists in the form of $UO_{2(s)}$, while U(VI) is in the form of soluble uranyl (UO_2^{2+}) and uranyl carbonate ions, which is generally much less mobile than U(VI) in the environment (Choppin et al. 2013; Mkandawire 2013; Newsome et al. 2014).

ZVI, a strong reducing agent, has been widely applied to treat wastewater with metals such as Pb^{2+}, UO_2^{2+}, etc. (Li and Zhang 2007; Sun et al. 2014). Previous studies have revealed that U(IV) can be removed by ZVI via reductive precipitation or adsorption onto corrosion products such as hematite (α-Fe_2O_3), geothite (α-FeOOH), and magnetite (Fe_3O_4)

The original article was revised: The original publication of this paper contains a mistake. The correct figure 7 is presented in this paper.

Responsible editor: Bingcai Pan

✉ Wenfa Tan
nhwftan@163.com

[1] Key Discipline Laboratory for National Defense of Biotechnology in Uranium Mining and Hydrometallurgy, University of South China, Hengyang 421001, China

[2] School of Resource Environment and Safety Engineering, University of South China, Hengyang 421001, China

[3] Hengyang Key Laboratory of Soil Pollution Control and Remediation, University of South China, Hengyang 421001, China

(Abdelouas 2006; Duan et al. 2018). Santos-Francés et al. (2018) found that Fe(II) may show a strong reducibility during the reduction of U(VI) through redox potential measurement. However, the corrosion products may in turn interferes with the reduction process. Scott et al. (2005) provided evidence that the pre-existent oxide film or the corrosion products prevent the subsequent interactions between ZVI and U(VI) during the U removal process. In addition, the reduction and adsorption rate of U(VI) by ZVI are contingent upon environmental conditions. Fiedor et al. (1998) determined the oxidation state of U(VI) on the surface of Fe by X-ray photoelectron spectroscopy. The results show that U(VI) was quickly adsorbed on ZVI and its oxides under aerobic conditions, while U(VI) was slowly and partly reduced to U(IV) under anaerobic conditions. Even though the chemical and physical processes of reducing U(VI) to U(IV) under different environmental conditions such as pH, temperature, and contact time have been well investigated (Li et al. 2016; Liu et al. 2019a), relatively little is known about the bio-mediated processes that influence the fate of U(VI) in aqueous solutions.

Bacteria are distributed widely in groundwater/water-bearing soil layer, which can affect the distribution and transformation of U(VI), Fe, and other metals through assimilation, alienation, and changing environmental conditions (Choudhary and Sar 2015; Xie et al. 2017). Therefore, bacteria may play a significant (positive or negative) role in treating U(VI)-contaminated water by ZVI. It has been reported that ZVI has selectivity when coexisting with microbiome (Kirschling et al. 2010; Xie et al. 2017). For example, nanometer ZVI has a certain toxic effect on the culture of bacteria, such as *Escherichia coli*, *Pseudomonas fluorescens*, and *Bacillus subtilis* (Fajardo et al. 2012). In addition, it is reported that *Bacillus subtilis* could significantly improve the adsorption rate of U(VI) by nanometer ZVI under the condition of high pH (Ding et al. 2015).

In our previous study (Ding et al. 2018), a purified indigenous bacteria (*Leifsonia* sp.) was isolated and showed excellent U(VI) adsorption property. The current study aims to: (1) investigate the effect of *Leifsonia* sp. on the removal efficiency of U(VI) by ZVI under varying environmental conditions, such as different dosage, contact time, pH, and initial U(VI) concentration and (2) identify the influence of *Leifsonia* sp. on removal mechanisms and stability of U–Fe precipitates. This study can provide theoretical reference for potential treatment of U(VI)-contaminated subsurface water via ZVI combined with *Leifsonia* sp.

Materials and methods

Bacteria, cultivation conditions and reagents

In our previous works, *Leifsonia* sp. was separated from acidic (pH 6~7) U(VI) tailing which was collected from tailings pond near Hengyang City, China (Ding et al. 2018). It has been found that the removal rate of U(VI) could reach 98% by *Leifsonia* sp. over the treatment ranges investigated. In this study, the third-generation *Leifsonia* sp. was cultured in aseptic beef extract peptone medium (3 g L^{-1} beef extract, 10 g L^{-1} peptone, 5 g L^{-1} NaCl), and then sub-packed bacterial fluid in 10 mL sterilized test tubes and kept in − 20 °C refrigerator. The bacteearium was activated by following steps: (1) the thawed *Leifsonia* sp. (10 mL) was added to the 250-mL medium in the sterile environment and incubated in the constant temperature shaker at 30 °C for 48 h (until the suspension became obviously cloudy); (2) in order to avoid the interference of culture medium, the activated *Leifsonia* sp. liquid was divided into 40 mL centrifuge tubes for centrifugation and washed with sterile deionized water for three times for later use.

Analytical grade or the highest purity chemicals without further purification were used. The solution pH was adjusted by 0.1 M NaOH and 0.1 M HNO_3. U(VI) stock solution (1 g L^{-1}) was obtained by dissolving U_3O_8 into concentrated nitric acid at 150 °C, and then diluted to the desired concentration.

Batch U(VI) removal experiment

A series of experiments were carried out to investigate the effect of *Leifsonia* sp. on the removal of U(VI) by ZVI. In the *Leifsonia* sp. experiments group, the initial concentration of the bacterium was maintained at 0.06 mg L^{-1}, and the reaction was carried out at 30 °C with an oscillating speed of 150 rpm. The sorption experiment was conducted through the following process: (1) U(VI)-simulated solution used in this work was prepared by diluting the stock solution to the desired concentration (10 mg L^{-1}); (2) 100 mL of 10 mg L^{-1} U(VI) solution, 0.006 mg collected *Leifsonia* sp., and 0.1 g ZVI powder were successively added and mixed in a 200-mL Erlenmeyer flask; (3) the initial pH was adjusted by adding 0.1 M NaOH and 0.1 M HNO_3; (4) the Erlenmeyer flask were placed in a shaking bath for contact reaction; and (5) when the entire adsorption system was equilibrated, the supernatant was filtered through 0.45 μm microporous membrane after centrifugation at 8000 rpm for 8 min. The residual U(VI) concentration was measured by T6 UV-vis spectrophotometry (Pgeneral, China) with Arsenazo III (Dedkova et al. 2008) as an indicator at 652 nm. All adsorption experiments were conducted in ambient condition.

In order to clarify the adsorption mechanism of U(VI), the dosage of ZVI was set at 0.05, 0.1, 0.5, 1, and 1.5 g L^{-1}. The pH range was fixed from 3 to 8. The contact time was set to be ~ 72 h. The initial U(VI) concentrations were 2.5, 5, 7.5, 10, and 20 mg L^{-1}. All experimental data were averaged from three independent measurements, and 5% error bars were provided.

The removal efficiency R(%) and adsorption capacity Q (mg g^{-1}) were calculated using the following formulas:

$$Q = \frac{(C_0 - C_e)V}{m} \quad (1)$$

$$R(\%) = \frac{(C_0 - C_e)}{C_0} \times 100\% \quad (2)$$

where C_0 and C_e (mg g^{-1}) denote the initial and final concentrations of U(VI), respectively, V (L) denotes the volume of solution, and m (g) denotes the mass of solid particles.

Desorption experiment

The desorption of U(VI) from ZVI-U(VI) and ZVI-*Leifsonia* sp.-U(VI) soil precipitation were investigated by using different desorbing agents (such as 0.1 M HNO_3 and 0.1 M Na_2CO_3). Based on the references (Duff et al. 2002; Li et al. 2015; Mason et al. 1997), 0.1 g sample was added into 100 mL 0.1 M desorption reagent and oscillated continuously for 2 h. The mixtures were filtered by 0.45 μm microporous membrane after centrifugation at 8000 rpm for 8 min. The concentration of U(VI) in desorbing solution was tested by the aforementioned method and spent adsorbent was washed with deionized water. All experiments were repeated for three times.

Formula (3) was generally used to calculate the desorption rate $D(\%)$:

$$D(\%) = \frac{C_D \times V_D}{Q_e \times m} \times 100\% \quad (3)$$

where C_D and V_D denote the concentration of U(VI) in the filtrate (mg L^{-1}) and the volume of desorption fluid (L), respectively.

Characterization

The collected precipitation was dried at 60 °C (ZVI) and freeze dried (Freeze Dryer, FD5-series) (ZVI + *Leifsonia* sp.), respectively. This sediment samples were analyzed by SEM-EDS, Fourier transform infrared spectroscopy (FTIR), X-photoelectron spectroscopy (XPS), and X-ray diffraction (XRD). The surface characteristics of ZVI, *Leifsonia* sp., and ZVI + *Leifsonia* sp. after interaction with U(VI) were observed by SEM (Zeiss SUPRATM55, Germany). And the distribution of elements after reaction was detected by EDS (Oxford-AztecX-Max80, UK). Infrared spectra in the range of 400–4000 cm^{-1} was recorded by FTIR (Bruker, Germany). XRD patterns of U(VI)-loaded samples were recorded by a diffractometer (Bruker D8 ADVANCE, Germany) with Cu-K_α radiation (40 kV, 40 mA) in a continuous scanning mode, and the 2θ scanning ranged from 10° to 90°. Jade6 software was used to analyze the U(VI) mineralization precipitation process and match the molecular formula. The XPS spectra were obtained by XPS (Thermo Fisher Scientific, USA) and the binding energies of U, Fe, and other elements were determined, through the radiation of Al-K_α. The XPS spectra of all elements were calibrated by C 1s peak at 284.6 eV.

Results and discussion

Effect of sorbent dose

The adsorption of U(VI) onto ZVI and ZVI + *Leifsonia* sp. were studied by varying the adsorbent quantity (0.05–1.5 g L^{-1}) in solution while keeping the constant initial U(VI) concentration (10 mg L^{-1}), temperature (30 °C) and pH (5) for 48 h equilibrium time. Figure 1 shows the plot of equilibrium adsorption capacity (mg g^{-1}) and U(VI) removal efficiency (%) against adsorbent dose (g L^{-1}) of ZVI and ZVI + *Leifsonia* sp., respectively. Obviously, the U(VI) removal efficiency increased with the increase of the dosage generally due to more binding sites available (Gok and Aytas 2009; Hua et al. 2012). The removal efficiency of U(VI) by ZVI increased from 85.15 to 93.75% when the dosage of ZVI increased from 0.05 to 0.5 g L^{-1}. However, when the dosage of ZVI was increased to 1 g L^{-1}, the U(VI) removal efficiency maintained at the near constant (97.64%). The removal of U(VI) by ZVI + *Leifsonia* sp. also shows the same trend. On the contrary, the adsorption capacity was decreased with the increase of the dosage within the scope of the experiment because of the competition for UO_2^{2+}. The reason might be due to the particle interaction, such as aggregation resulting from high adsorbent dose of ZVI. Such aggregation would lead to the decrease of total surface area of ZVI and the increase in diffusional path length. Notably, compared with the controlled group, the U(VI) removal efficiency was slightly increased by adding *Leifsonia* sp when the dose of ZVI was less than 1 g L^{-1}. This demonstrates that *Leifsonia* sp. changed

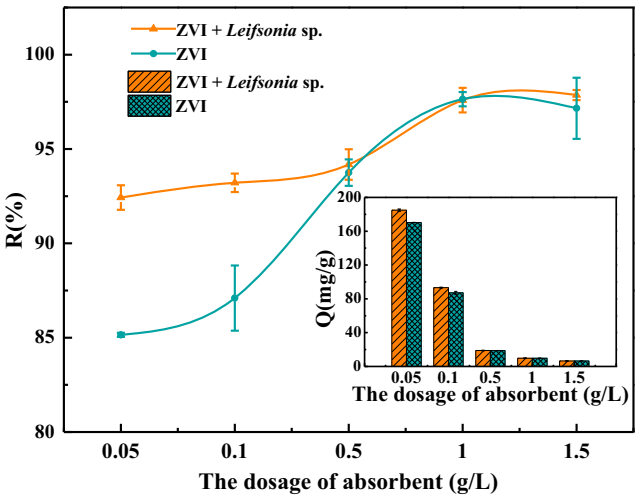

Fig. 1 Effect of sorbent dose of ZVI and ZVI + *Leifsonia* sp. on removal of U(VI) under pH = 5, T = 30 °C, contact time = 48 h, initial *Leifsonia* sp. of 0.06 mg L^{-1}, and initial U(VI) concentration of 10 mg/L (n = 3)

the interaction between ZVI and U, i.e., covering on the surface of ZVI.

Effect of contact time

The influence of contact time (~ 72 h) on the removal of U(VI) by ZVI and ZVI + *Leifsonia* sp. were studied, respectively. Figure 2a shows that the adsorption process of U(VI) by ZVI was relatively fast in the first 1.5 h and reached the steady level on 2 h with the removal rate of 97.91 %. The decrease in removal rate is attributed to the decrease in available active sites and the slower diffusion of U(VI) ions from the adsorbent surface to the internal structure (Duan et al. 2019). Comparatively speaking, Fig. 2b shows that the adsorption process of U(VI) by ZVI + *Leifsonia* sp. was much slower than that of ZVI only. Over the treatment ranges investigated, the adsorption capacity reached the maximum value after 48 h in the presence of *Leifsonia* sp. The adsorption capacity of U(VI) by ZVI + *Leifsonia* sp. reached 9.79 mg g^{-1} after 48 h, which is higher than that of ZVI (8.2 mg g^{-1}). The increased removal capacity of U(VI) on ZVI+ *Leifsonia* sp. may due to the increased sorption sites and the functional groups on *Leifsonia* sp. It is well known that U(VI) removal processes may depend on and be controlled by different types of mechanisms. Biological action, i.e., biosorption, bioreduction, and biomineralization (Wang et al. 2019), initiative adsorption is much slower than chemical or physical absorption. All these indicate that *Leifsonia* sp. played an important role in the reaction.

Effect of pH

Figure 3 shows the adsorption of U(VI) onto the ZVI and ZVI + *Leifsonia* sp. under different pH values. The removal rate and adsorption capacity of U(VI) were investigated by ZVI and ZVI + *Leifsonia* sp. at different pH values (3, 4, 5, 6, 7, and 8). As shown in Fig. 3, the

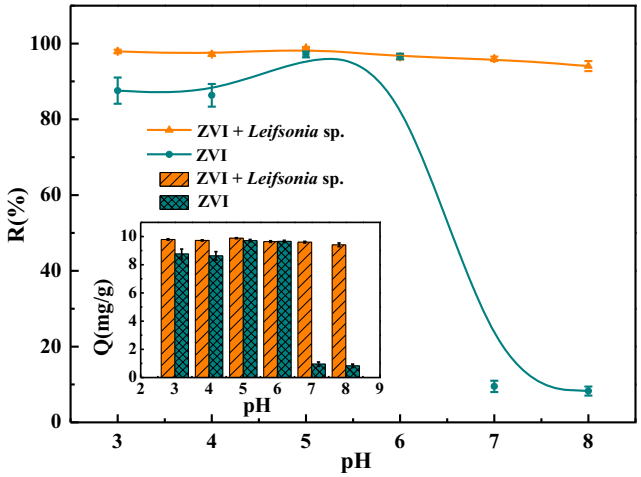

Fig. 3 Effect of pH on U(VI) removal. T = 30 °C, contact time 48 h, ZVI dosage 1 mg L^{-1}, initial *Leifsonia* sp. of 0.06 mg L^{-1}, and initial U(VI) concentration of 10 mg L^{-1} (n = 3)

removal rate of U(VI) by ZVI increased when the pH increased from 3 to 5 and the maximum adsorption capacity achieved 9.63 mg g^{-1} at pH value of 5 over the treatment ranges investigated. Yet, the adsorption capacity decreased rapidly from 96.58 to 9.5% with the further elevation of pH due to the generation of stable uranium carbonate complex-like $UO_2(CO_3)_2^{2-}$ and $UO_2(CO_3)_3^{4-}$ (Song et al. 2014). It was found that the U(VI) adsorption first increased within the pH of 3 to 5, and then maintained constant from pH 5 to 6. This reveals that ZVI has good adsorption performance only under acidic and near-neutral conditions. UO_2^{2+} is the predominant species of U(VI) at the pH (3~5), which can compete with H^+ ions for the binding sites on the surface of adsorbents, leading to the low removal rate. At pH 5 to 6, UO_2^{2+} is partially hydrolyzed to form other uranium species, such as $[(UO_2)_3(OH)_5]^+$, $[(UO_2)_2(OH)_2]^{2+}$, and $[UO_2(OH)]^+$ (Liu et al. 2017). It was found that U(VI) mainly existed in the presence of UO_2^{2+} at pH of 3~5. ZVI has strong adsorption capacity of UO_2^{2+} at the pH scope (Klas and Kirk

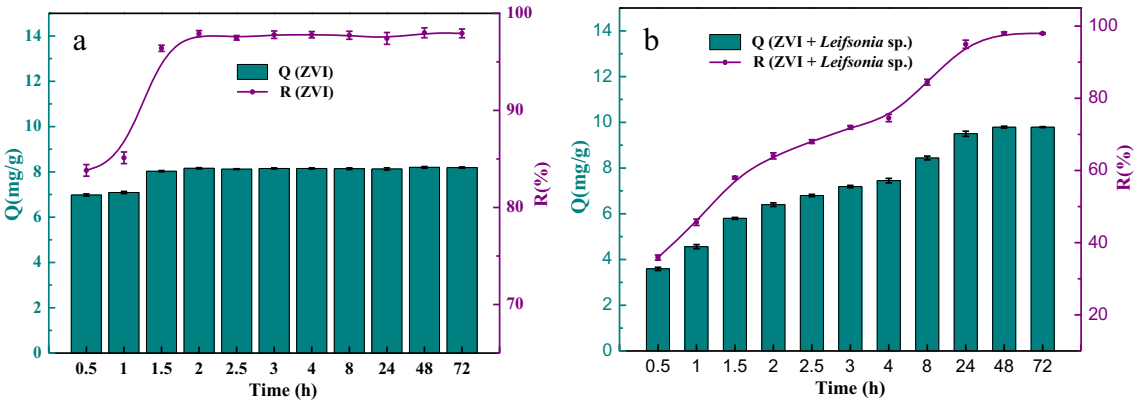

Fig. 2 Effect of contact time on U(VI) fixation by ZVI (**a**) and ZVI + *Leifsonia* sp. (**b**). pH = 5, T = 30 °C, ZVI dosage of 1 g L^{-1}, initial *Leifsonia* sp. of 0.06 mg L^{-1}, and initial U(VI) concentration of 10 mg L^{-1} (n = 3)

2013; Peng et al. 2017). When pH > 6, U(VI) is dominant in the presence of more complexes such as uranyl hydroxyl complexes and polynuclear uranyl hydroxyl complexes, and the reactivity of ZVI is greatly inhibited (Korichi and Bensmaili 2009; Zhao et al. 2012). Although, the chemical bonding between structural Fe(II) or Fe(III) of ZVI altered with increasing pH (especially at pH > 3.8). Notably, in the presence of *Leifsonia* sp., the removal rates of U(VI) were not significantly altered when the initial pH increased from 3 to 8. The removal rates of U(VI) were maintained at high levels (over 90 %) within the experimental scope, which can be attributed to the increased sorption sites and the functional groups of *Leifsonia* sp.

Effect of the initial U(VI) concentration

The effect of different initial U(VI) concentration (2.5, 5, 7.5, 10, and 20 mg L^{-1}) on removal efficiency was investigated. The results in Fig. 4 show that the removal rate was more than 96.83% as the initial U(VI) concentration increased from 2.5 to 10 mg L^{-1}. While the removal ratio decreased by 30.38% (for ZVI) and 27.18% (for ZVI + *Leifsonia* sp.), respectively, when U(VI) concentration increased to 20 mg L^{-1}. This may be due to the saturation of ZVI adsorption capacity. As the concentration of U(VI) increases, UO_2^{2+} ions compete for adsorption sites or available functional groups (Yousef et al. 2019). However, the adsorption capacity continues to increase with the rise of initial U(VI) concentration, which is due to the presence of more U(VI) ions around ZVI (Feng et al. 2011). The maximum capacity were up to 10.4 mg g^{-1} (ZVI + U(VI)) and 14.29 mg g^{-1} (ZVI + *Leifsonia* sp. + U(VI)) at the initial U(VI) concentration of 20 mg L^{-1}.

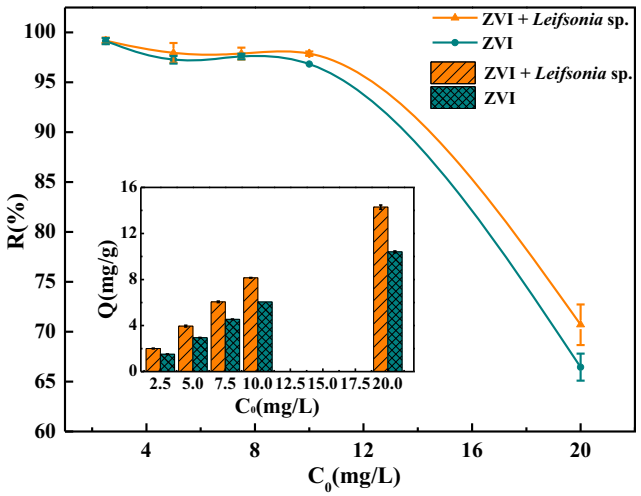

Fig. 4 Effect of initial U concentration on U(VI) removal. T = 30 °C, contact time = 48 h, ZVI dosage = 1 mg L^{-1}, and initial *Leifsonia* sp. of 0.06 mg L^{-1} (n = 3)

Adsorption kinetics

Adsorption kinetics is an important model for evaluating the removal efficiency of U(VI). The kinetic investigation was conducted over the contact time range of 0~72 h. The pseudo-first- and pseudo-second-order kinetic equations were applied to describe the kinetic characteristics of U(VI) onto the ZVI + *Leifsonia* sp.. The pseudo-first- and the pseudo-second-order kinetic equation are shown in Eqs. (4) and (5), respectively:

$$Q_t = Q_e \times \left(1 - e^{-k_1 t}\right) \tag{4}$$

$$Q_t = \frac{k_2 Q_e^{\,2} t}{1 + k_2 Q_e t} \tag{5}$$

where Q_e and Q_t denote the adsorption amount at equilibrium and at any time (mg g^{-1}), respectively. In addition, k_1 denotes the equilibrium rate constant of pseudo-first-order sorption (1/min) and k_2 denotes the equilibrium rate constant of pseudo-second-order sorption (g mg^{-1} min^{-1}).

In order to further explore the adsorption mechanism of the reaction process, pseudo-first- and pseudo-second-order models were used to fit the experimental data. The fitting results are shown in Fig. 5 and Table 1. It can be observed from the kinetic plots that both pseudo-first- and pseudo-second-order rate expressions have a good agreement with the experimental data. However, it can be seen that the values of Pearson's r and R^2, coefficient of determination for the pseudo-second-order model are slightly higher than that of pseudo-first-order model. This indicates that the pseudo-second-order model can describe the sorption process better. These results are in accordance with Wang et al. (2010) and Sun et al. (2014). These results implied that sorption on ZVI is a complex process, which may be related to several mechanisms such as physical adsorption, chemisorptions, and reactions. Moreover, the $Q_{e,\ exp}$ value of ZVI + *Leifsonia* sp. is higher than that of ZVI, indicating that the addition of *Leifsonia* sp. enhanced the adsorption of U(VI) by ZVI.

Desorption efficiency

In order to evaluate the stability of the adsorbed precipitates of ZVI and ZVI + *Leifsonia* sp., desorption study of the precipitates with the highest U(VI) removal efficiency (96.27 and 97.34%) was carried out after the batch experiment. Previous studies revealed that HNO_3 and Na_2CO_3 inhibited the sorption and reduction of U(VI) (Ding et al. 2015; Li et al. 2013). The two products were desorbed in HNO_3 and Na_2CO_3 desorption solution, respectively. As shown in Fig. 6, the desorption efficiency of precipitates in group of ZVI + *Leifsonia* sp. under HNO_3 was higher than that of ZVI. In Na_2CO_3 desorption solution, the desorption rate of two groups were substantially

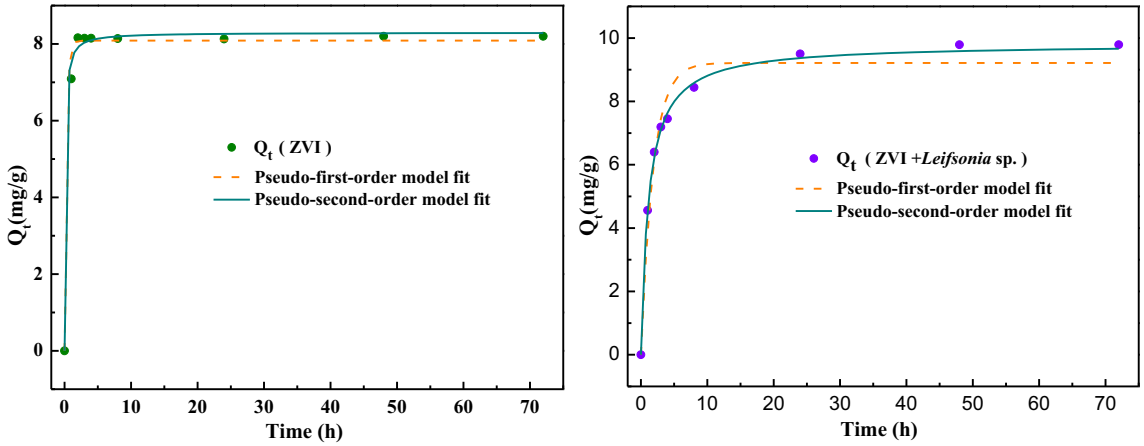

Fig. 5 Adsorption kinetics of U(VI) adsorption process by ZVI and ZVI + *Leifsonia* sp. pH = 5.0, T = 30 °C, ZVI dosage = 1 mg L^{-1}, initial *Leifsonia* sp. of 0.06 mg L^{-1}, and initial U(VI) concentration of 10 mg L^{-1} (n = 3)

similar. Liu et al. explained in their study that the absorption process was more difficult than the adsorption process, possibly because desorption required higher activation energy to break the strong bond between U and functional groups on the surface of the adsorbent (Liu et al. 2019b). It has been reported that U(VI) bound in iron oxide structure or blocked by iron oxide were not easily leached by carbonate (Duff et al. 2002). Notably, in ZVI, the desorption rate in HNO_3 is approximately 5.24% lower than that in Na_2CO_3, while in ZVI + *Leifsonia* sp., the desorption rate in HNO_3 is approximately 16.66% higher than that in Na_2CO_3. All these indicate that *Leifsonia* sp. participate, to some extent, in the adsorption process (Tan et al. 2018; Zheng et al. 2018).

SEM and EDS analysis

SEM micrographs and EDS analysis of ZVI, *Leifsonia* sp., and ZVI + *Leifsonia* sp. after U(VI) adsorption are shown in Fig. 7, respectively. As shown in Fig. 7, the typical SEM images of the precipitates exhibited some differences. Many particles were scattered on the surface of the ZVI, which were mostly spherical and sheet-like shape (Fig. 7a). These may be the deposition of corrosion products of ZVI and U(VI) oxides, respectively (Li et al. 2015; Riba et al. 2008). It has been demonstrated that the surface of *Leifsonia* sp. was wrinkled and rough, may be due to dehydration (Fig. 7b). The nanoparticles on the surface of the cells appear to be uranium crystals (Jialin 2015). It has been reported that microbial organisms can interact with U(VI) to form phosphate mineral precipitates (Salome et al. 2013). When *Leifsonia* sp. was added into ZVI + U(VI) system, yellow precipitate was found gradually. These results indicate that *Leifsonia* sp. played a role in the process. And dense scaly precipitates were clearly observed on the samples (Fig. 7c). Phosphorus and U(VI) elements were found in the EDS spectra (Fig. 7f), combined with previous researchers, i.e., Wang et al. (2017), the precipitates may be considered uranyl-phosphate minerals (Huang et al. 2017; Liu et al. 2010). It can be seen that no peaks of U was observed due to its low concentration (Fig. 7d, e).

FTIR analysis

The absorption of organometallic compounds in 4000–600 cm^{-1} is mainly caused by the vibration of the coordination group, and the metal elements have no influence on the characteristic absorption of the coordination group (Korichi and Bensmaili 2009). The variations in the structure and surface functional groups after ZVI immobilization of U(VI) with and without the addition of *Leifsonia* sp. were systematically investigated using infrared spectroscopy, as shown in Fig. 8.

For ZVI-added group, the strong peaks near 3398 and 2906 cm^{-1} are assigned to the stretching vibration of –OH group. The vibration peaks at 1733 and 1650 cm^{-1} are attributed to C=O. And the characteristic band at 896 cm^{-1} is attributed to Fe–O–H bending vibration. Compared with ZVI + *Leifsonia* sp.-added group, as shown in Fig. 8, structure and surface

Table 1 Fitting parameters of pseudo-first-order and pseudo-second order kinetic models of ZVI + *Leifsonia* sp. (n = 3)

Sorbent	$Q_{e,\ exp}$ (mg g^{-1})	K_1 (min^{-1})	Pseudo-first-order model			K_2 (g mg^{-1} min^{-1})	Pseudo-second-order model		
			Q_e (mg g^{-1})	Pearson's r	R_1^2		Q_e (mg g^{-1})	Pearson's r	R_2^2
ZVI	8.20	3.55 ± 0.39	8.09 ± 0.09	0.694	0.987	1.24 ± 0.23	8.29 ± 0.09	0.890	0.992
ZVI + *Leifsonia* sp.	9.79	0.55 ± 0.07	9.22 ± 0.28	0.591	0.967	0.09 ± 0.01	9.817 ± 0.1	0.746	0.997

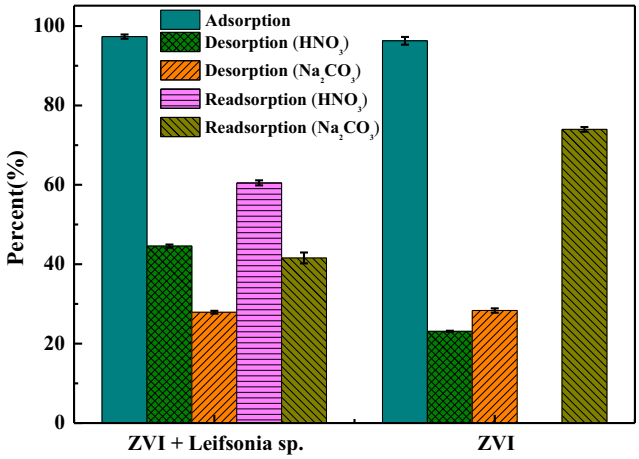

Fig. 6 Desorption proportion of the adsorbed U precipitates under 0.1 M HNO_3 and 0.1 M Na_2CO_3 for 2 h, respectively (n = 3)

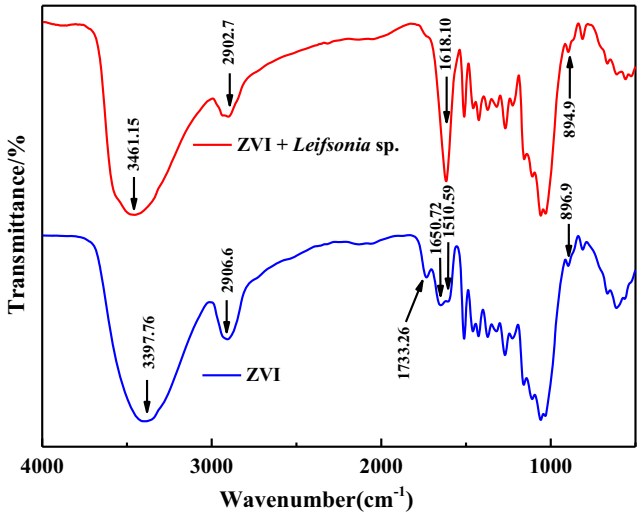

Fig. 8 The FTIR spectra of ZVI and ZVI + *Leifsonia* sp. contacted with 10 mg L^{-1} U(VI). ZVI = 1 g L^{-1}, pH = 5, T = 30 °C, and t = 48 h

functional groups were shifted. The peak of –OH stretching and bending vibration at 3398 cm^{-1} shift to 3461 cm^{-1}. In addition, the vibration peaks disappeared at 1733 and 1650 cm^{-1} and a new vibration peak appeared at 1618 cm^{-1}. All these results indicate that functional groups on the surface of *Leifsonia* sp. may be involved in the process.

XPS analysis

The XPS of ZVI and ZVI + *Leifsonia* sp. after the U(VI) adsorption could provide the evidences of chemical elements of uranium, iron, and oxygen, and the adsorptive evidence of UO_2^{2+} ions on ZVI and *Leifsonia* sp. The full-scan XPS spectra of ZVI and ZVI + *Leifsonia* sp. after reaction with U(VI) are shown in Fig. 9a. A high-resolution XPS patterns of C 1s, O 1s, N 1s, Fe 2p, U 4f, and P 2p of ZVI and ZVI + *Leifsonia* sp. particles after reaction are shown in Fig. 9. It can be shown that the N 1s, U 4f, and P 2p peaks are weak due to low concentrations.

The C 1s peaks (Fig. 9b) can be decomposed into the following three components: peak 1 (C–C/H) at 284.6 eV, peak 2 (C–O, C–N) at 286.11 eV, and peak 3 (C=O, –COOH) at 288.35 eV (Zhang et al. 2018b). By contrast, the binding energies of C–O, C–N, and C=O, –COOH groups were reduced by 0.11 and 0.27 eV for sample ZVI + *Leifsonia* sp. The results showed that the groups involved in uranium reaction belong to oxygen-containing functional groups (Liu et al. 2019a). In Fig. 9c, O 1s spectrum can be determined as three peaks, which are attributed to O^{2-} (531.78 eV), C=O (530.58

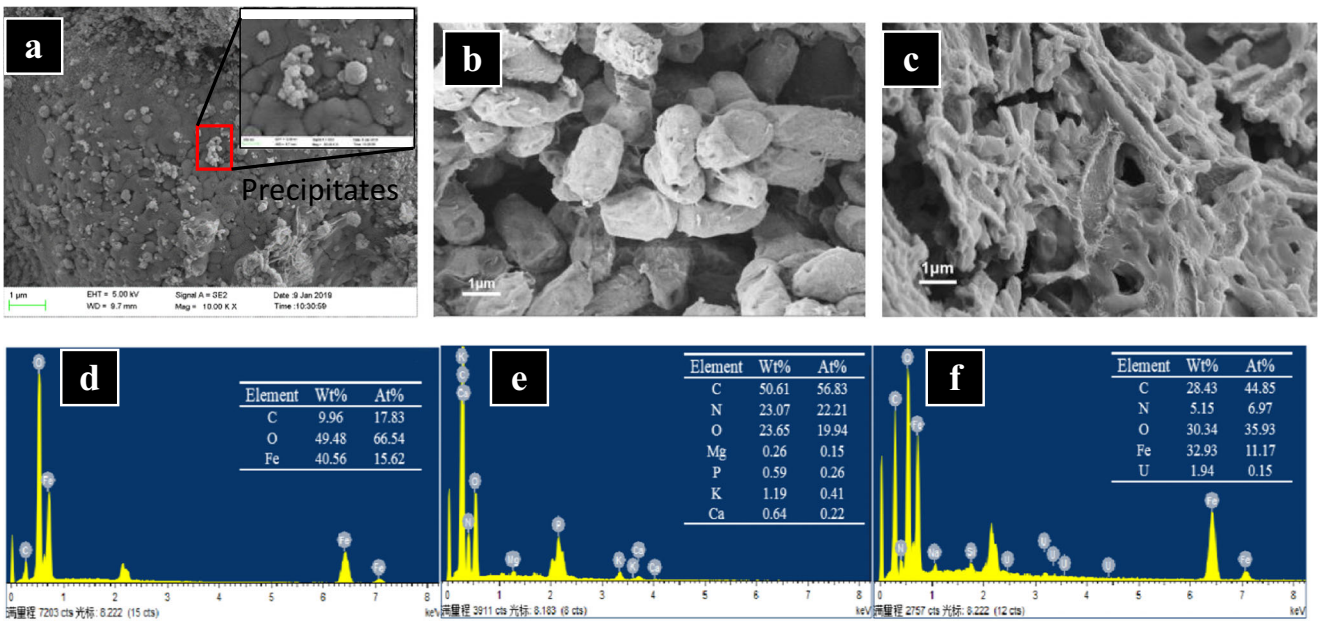

Fig. 7 The characterization of SEM images and EDS analysis of ZVI (**a**, **d**), *Leifsonia* sp. (**b**, **e**), and ZVI + *Leifsonia* sp. (**c**, **f**). U(VI) = 10 mg L^{-1}, pH = 5, t = 48 h, and ZVI dosage = 1 g L^{-1}. Illustration is an enlarged image of the load

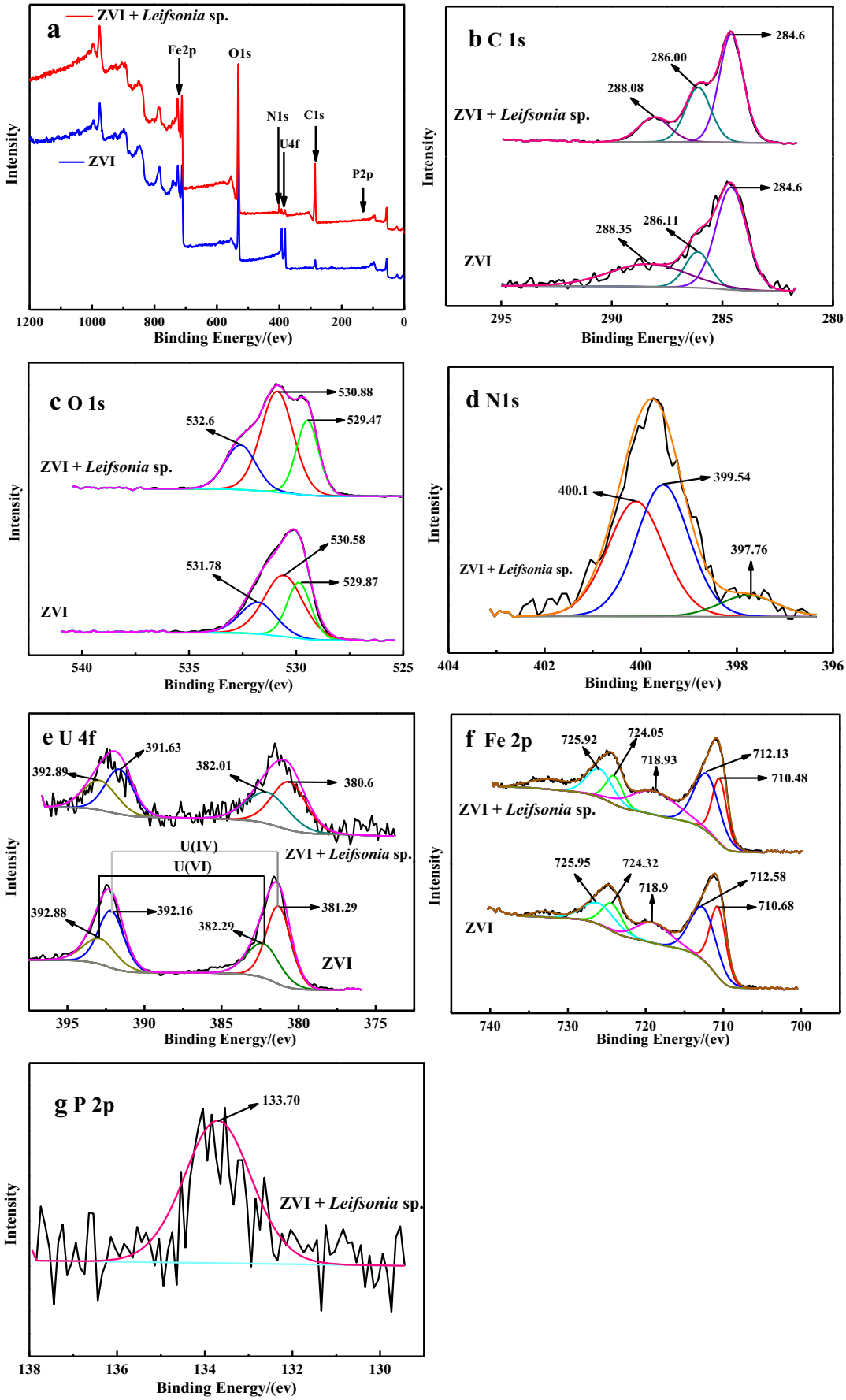
a
ZVI + Leifsonia sp.
ZVI
Fe2p
O1s
N1s
C1s
U4f
P2p
Intensity
Binding Energy/(ev)
b C 1s
284.6
286.00
288.08
ZVI + Leifsonia sp.
284.6
286.11
288.35
ZVI
c O 1s
530.88
532.6
529.47
ZVI + Leifsonia sp.
530.58
531.78
529.87
ZVI
d N1s
399.54
400.1
397.76
ZVI + Leifsonia sp.
e U 4f
391.63
392.89
382.01
380.6
U(IV)
U(VI)
ZVI + Leifsonia sp.
392.88
392.16
381.29
382.29
ZVI
f Fe 2p
725.92
724.05
718.93
712.13
710.48
ZVI + Leifsonia sp.
725.95
724.32
718.9
712.58
710.68
ZVI
g P 2p
133.70
ZVI + Leifsonia sp.

◀ **Fig. 9** X-ray photoelectron binding energy curves of ZVI and ZVI + *Leifsonia* sp.: **a** full spectrum, **b** C 1s spectra, **c** O 1s spectra, **d** N 1s spectra, **e** U 4f spectra, **f** Fe 2p spectra, and **g** P 2p spectra. U(VI) = 10 mg L^{-1}, ZVI = 1 g L^{-1} (biomass = 0.06 g L^{-1}), pH = 5, 30 °C, and t = 48 h

eV), and O–H (529.87 eV) bonds, respectively (Liu et al. 2014). After the addition of *Leifsonia* sp., the binding energies of O 1s were all shifted. It is noteworthy that the N 1s spectrum was detected after the addition of *Leifsonia* sp. (Fig. 9d). And it can be divided into three peaks with the binding energy at 397.76, 399.54, and 400.1 eV, respectively, which are classified as C–N, C=N, and NH_3-functional group (Zhang et al. 2018a). It can be inferred that N supplied by *Leifsonia* sp. is contributing to the removal of U(VI).

As shown in Fig. 9e, the detailed U 4f spectrum concentrated on 381.29 and 392.16 eV proved the existence of U(IV) phase, and the double peaks of U 4f located at 382.29 and 392.88 eV indicated the occurrence of the reduction state of U(VI) (Liu et al. 2015). The fitting curve of U $4f_{7/2}$ and U $4f_{5/2}$ peaks clearly show the relative proportion between U(VI) and U(IV) on the sample surface. The existence of the U(VI) species is owing to the chemical adsorption of U(VI). However, the presence of U(IV) on the surface of the sample is a result of iron redox. In the XPS spectra of Fe 2p (Fig. 9f), the Fe 2p peaks displayed broad Fe $2p_{3/2}$ and Fe $2p_{1/2}$ lines located at 710.68 ± 0.2 and 724.32 ± 0.2 eV, respectively, which can be attributed to surface Fe(II)/Fe(III)-bearing oxides including Fe_3O_4 and FeO(OH), as reported in previous works (Missana et al. 2003). The Fe $2p_{3/2}$ for Fe^0 had satellite peaks at 718.90 eV. In the presence and absence of *Leifsonia* sp., Fe peaks can always be detected on the surface of ZVI after reaction with U(VI). It can be inferred that ZVI can continuously provide electrons in the reaction process because the oxide layer protects the Fe^0 core (Li and Zhang 2007). Meanwhile, the presence of Fe(III) revealed that Fe(II) could reduce U(VI). Notably, as shown in Fig. 9g, P 2p peak was observed at 133.34 eV in the ZVI + *Leifsonia* sp. system, which may be attributed to PO_4^{3-} released by *Leifsonia* sp..

XRD analysis

The XRD patterns of the ZVI and ZVI + *Leifsonia* sp. after reaction are shown in Fig. 10. XRD analysis shows that metallic iron was the main phase. ZVI corrosion products are mainly magnetite (Fe_3O_4) and maghemite (γ-Fe_2O_3) (Li et al. 2015). The characteristic peaks appeared at 30.09°, 35.52°, 44.67°, 57.17°, 62.86°, 65.03°, and 82.33° after adsorption (ZVI, ZVI + *Leifsonia* sp.). These 2-theta values have good correlation with the lepidocrocite (FeO(OH) PDF No. 08-0098), magnetite (Fe_3O_4 PDF No. 88-0315), iron Fe (Fe PDF No. 06-0696), and maghemite (Fe_2O_3 PDF No. 39-1346), comparing with data files of known compounds. In addition, the intensities of magnetite peaks in the ZVI +

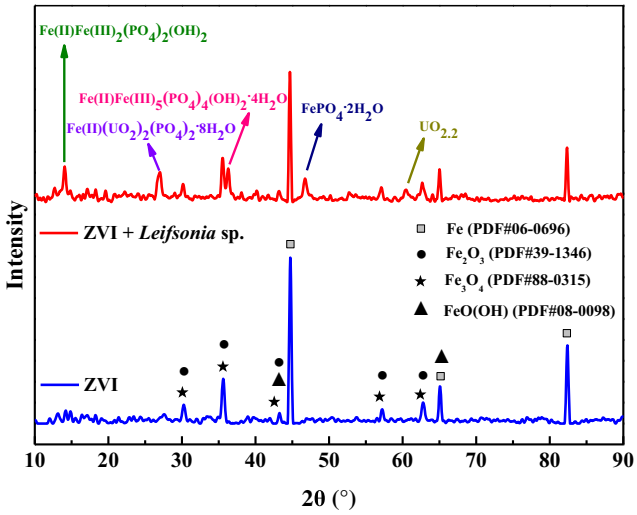

Fig. 10 XRD patterns of the precipitation products of ZVI and ZVI + *Leifsonia* sp. U(VI) = 10 mg L^{-1}, ZVI = 1 g L^{-1}, pH = 5, T = 30 °C, and t = 48 h

Leifsonia sp. group were lower than that in the ZVI group, indicating that the presence of *Leifsonia* sp. may inhibit the corrosion of ZVI. These peaks do not correspond exactly to any type of U(VI) mine, which are similar to the results obtained by Qiu et al. (2001). New characteristic peaks appeared for ZVI + *Leifsonia* sp. at 14.05°, 27.06°, 46.66°, and 60.56°, and the theoretical results fit well with barbosalite $(Fe(II)Fe(III)_2(PO_4)_2(OH)_2$ PDF No. 33-0668), bassetite $(Fe(II)(UO_2)_2(PO_4)_2{\cdot}8H_2O$ PDF No. 07-0288), beraunite $(Fe(II)Fe(III)_5(PO_4)_4(OH)_2{\cdot}4H_2O$ PDF No. 22-0631), strengite ($FePO_4{\cdot}2H_2O$ PDF No. 33-0667), and uraninte-O ($UO_{2.2}$ PDF No. 47-1879). The results showed that the presence of *Leifsonia* sp. promoted the formation of UO_2, bassetite, and beraunite, which may be related to the phosphoric groups produced by the cells combined with the XPS data. Its morphological features are also well presented in Fig. 7c.

Conclusion

This study compares the removal efficiency and mechanisms by ZVI in the presence and absence of *Leifsonia* sp. The results showed that the removal rate and capacity of U(VI) was significantly inhibited and decreased by ZVI under near-neutral condition. However, in the ZVI + *Leifsonia* sp. coexistence system, the U(VI) removal efficiency of U(VI) were maintained at high levels (over 90.00%) within the experimental scope, which can be attributed to the increased sorption sites and the functional groups of *Leifsonia* sp. And the kinetics analyses indicated that *Leifsonia* sp. participated in the adsorption process. Meanwhile, mechanism analyses showed that the dense scaly uranium-phosphate precipitation was observed on the ZVI + *Leifsonia* sp. surface. New substances, barbosalite $(Fe(II)Fe(III)_2(PO_4)_2(OH)_2)$, bassetite

($Fe(II)(UO_2)_2(PO4)_2 \cdot 8H_2O$), beraunite ($(Fe(II)Fe(III)_5(PO_4)_4(OH)_2 \cdot 4H_2O$), etc., were produced in the presence of *Leifsonia* sp. All these results revealed that there are synergistic effects in the presence of *Leifsonia* sp. Therefore, coupled ZVI and *Leifsonia* sp. might be potentially exploited in the bioremediation of U(VI)-contaminated environment in situ.

Funding information The authors gratefully acknowledge the financial support by the National Natural Science Foundation of China (No. 11605087 and No. 11475080), China's Post-doctoral Science Fund (No. 2017M610500), and the Natural Science Foundation of Hunan Province, China (No. 2019JJ50513). All the support is greatly appreciated.

Compliance with ethical standards

Conflict of interest The authors declare that they have no conflict of interest.

References

Abdelouas A (2006) Uranium mill tailings: geochemistry, mineralogy and environmental impact. Elements 2:335–341

Basu H, Singhal RK, Pimple MV, Reddy AVR (2015) Synthesis and characterization of silica microsphere and their application in removal of uranium and thorium from water. Int J Environ Sci Technol 12:1899–1906

Černe M, Smodiš B, Štrok M, Jaćimović R (2018) Plant accumulation of natural radionuclides as affected by substrate contaminated with uranium-mill tailings. Water Air Soil Pollut 229:1–21

Choppin G, Liljenzin JO, Rydberg J, Ekberg C (2013) Chapter 22: Behavior of radionuclides in the environment. Radiochem Nucl Chem 84:753–788

Choudhary S, Sar P (2015) Interaction of uranium (VI) with bacteria: potential applications in bioremediation of U contaminated oxic environments. Rev Environ Sci Biotechnol 14:1–9

Dedkova VP, Shvoeva OP, Savvin SB (2008) Sorption-spectrometric determination of thorium(IV) and uranium(VI) with the reagent Arsenazo III on the solid phase of a fibrous material filled with a cation exchanger. J Anal Chem 63:430–434

Ding C, Cheng W, Sun Y, Wang X (2015) Effects of Bacillus subtilis on the reduction of U(VI) by nano-Fe 0. Geochim Cosmochim Acta 165:86–107

Ding L, Tan WF, Xie SB, Mumford K, Lv JW, Wang HQ, Fang Q, Zhang XW, Wu XY, Li M (2018) Uranium adsorption and subsequent re-oxidation under aerobic conditions by Leifsonia sp.-Coated biochar as green trapping agent. Environ Pollut 242:778–787

Duan S, Xu X, Liu X, Wang Y, Hayat T, Alsaedi A, Meng Y, Li J (2018) Highly enhanced adsorption performance of U(VI) by non-thermal plasma modified magnetic Fe3O4 nanoparticles. J Colloid Interface Sci 513:92–103

Duan S, Wu L, Li J, Huang Y, Tan X, Wen T, Hayat T, Alsaedi A, Wang X (2019) Two-dimensional copper-based metal-organic frameworks nano-sheets composites: one-step synthesis and highly efficient U(VI) immobilization. J Hazard Mater 373:580–590

Duff MC, Coughlin JU, Hunter DB (2002) Uranium co-precipitation with iron oxide minerals. Geochim Cosmochim Acta 66:3533–3547

Fajardo C, Ortíz LT, Rodríguez-Membibre ML, Nande M, Lobo MC, Martin M (2012) Assessing the impact of zero-valent iron (ZVI) nanotechnology on soil microbial structure and functionality: a molecular approach. Chemosphere 86:802–808

Feng J, Liang C, Wang L, Zhang X (2011) Kinetics of Cr(VI) removal from aqueous solution with nanoscale zero-valent iron. Sci Technol Rev 29:37–41

Fiedor JN, Bostick WD, Jarabek RJ, Farrell J (1998) Understanding the mechanism of uranium removal from groundwater by zero-valent iron using X-ray photoelectron spectroscopy. Environ Sci Technol 32:1466–1473

Gok C, Aytas S (2009) Biosorption of uranium(VI) from aqueous solution using calcium alginate beads. J Hazard Mater 168:369–375

Hua C, Zhang R, Li L, Zheng X (2012) Adsorption of phenol from aqueous solutions using activated carbon prepared from crofton weed. Desalin Water Treat 37:230–237

Huang W et al (2017) Microscopic and spectroscopic insights into uranium phosphate mineral precipitated by Bacillus Mucilaginosus. ACS Earth Space Chem 1:483–492

Jialin MA (2015) The adsorption behavior on uranium by three kinds of microorganisms. China Environ Sci 35:825–832

Kirschling TL, Gregory KB, Minkley EG, Lowry GV, Tilton RD (2010) Impact of nanoscale zero valent iron on geochemistry and microbial populations in trichloroethylene contaminated aquifer materials. Environ Sci Technol 44:3474–3480

Klas S, Kirk DW (2013) Advantages of low pH and limited oxygenation in arsenite removal from water by zero-valent iron. J Hazard Mater 252:77–82

Korichi S, Bensmaili A (2009) Sorption of uranium (VI) on homoionic sodium smectite experimental study and surface complexation modeling. J Hazard Mater 169:780–793

Li XQ, Zhang WX (2007) Sequestration of metal cations with zero valent iron nanoparticles: a study with high resolution X-ray photoelectron spectroscopy (HR-XPS). J Phys Chem C 111:6939–6946

Li X, Wu J, Liao J, Zhang D, Yang J, Feng Y, Zeng J, Wen W, Yang Y, Tang J, Liu N (2013) Adsorption and desorption of uranium (VI) in aerated zone soil. J Environ Radioact 115:143–150

Li ZJ, Wang L, Yuan LY, Xiao CL, Mei L, Zheng LR, Zhang J, Yang JH, Zhao YL, Zhu ZT, Chai ZF, Shi WQ (2015) Efficient removal of uranium from aqueous solution by zero-valent iron nanoparticle and its graphene composite. J Hazard Mater 290:26–33

Li F et al (2016) Microorganism-derived carbon microspheres for uranium removal from aqueous solution. Chem Eng J 284:630–639

Liu M, Dong F, Yan X, Zeng W, Hou L, Pang X (2010) Biosorption of uranium by Saccharomyces cerevisiae and surface interactions under culture conditions. Bioresour Technol 101:8573–8580

Liu A, Liu J, Pan B, Zhang WX (2014) Formation of lepidocrocite (γ-FeOOH) from oxidation of nanoscale zero-valent iron (nZVI) in oxygenated water. RSC Adv 4:57377–57382

Liu JX, Xie SB, Wang YH, Liu YJ, Cai PL, Xiong F, Wang WT (2015) U(VI) reduction by Shewanella oneidensis mediated by anthraquinone-2-sulfonate. Trans Nonferrous Metals Soc China 25:4144–4150

Liu S, Yang Y, Liu T, Wu W (2017) Recovery of uranium(VI) from aqueous solution by 2-picolylamine functionalized poly(styrene-co-maleic anhydride) resin. J Colloid Interface Sci 497:385–392

Liu L, Liu J, Liu X, Dai C, Zhang Z, Song W, Chu Y (2019a) Kinetic and equilibrium of U(VI) biosorption onto the resistant bacterium Bacillus amyloliquefaciens. J Environ Radioact 203:117–124

Liu X, Sun J, Xu X, Alsaedi A, Hayat T, Li J (2019b) Adsorption and desorption of U(VI) on different-size graphene oxide. Chem Eng J 360:941–950

Mason CFV, Turney WRJR, Thomson BM, Lu N, Chisholm-Brause CJ (1997) Carbonate leaching of uranium from contaminated soils. Environ Sci Technol 31:2707–2711

Missana T, Maffiotte C, Garcia-Gutiérrez M (2003) Surface reactions kinetics between nanocrystalline magnetite and uranyl. J Colloid Interface Sci 261:154–160

Mkandawire M (2013) Biogeochemical behaviour and bioremediation of uranium in waters of abandoned mines. Environ Sci Pollut Res Int 20:7740–7767

Newsome L, Morris K, Lloyd JR (2014) The biogeochemistry and bioremediation of uranium and other priority radionuclides. Chem Geol 363:164–184

Peng X, Xi B, Zhao Y, Shi Q, Meng X, Mao X, Jiang Y, Ma Z, Tan W, Liu H, Gong B (2017) Effect of arsenic on the formation and adsorption property of ferric hydroxide precipitates in ZVI treatment. Environ Sci Technol 51:10100–10108

Qiu SR et al (2001) Characterization of uranium oxide thin films grown from solution onto Fe surfaces. Appl Surf Sci 181:211–224

Riba O, Scott TB, Ragnarsdottir KV, Allen GC (2008) Reaction mechanism of uranyl in the presence of zero-valent iron nanoparticles. Geochim Cosmochim Acta 72:4047–4057

Salome KR, Green SJ, Beazley MJ, Webb SM, Kostka JE, Taillefert M (2013) The role of anaerobic respiration in the immobilization of uranium through biomineralization of phosphate minerals. Geochim Cosmochim Acta 106:344–363

Santos-Francés F, Pacheco EG, Martínez-Graña A, Rojo PA, Sánchez AG (2018) Concentration of uranium in the soils of the west of Spain. Environ Pollut 236:1–11

Scott TB, Allen GC, Heard PJ, Randell MG (2005) Reduction of U(VI) to U(IV) on the surface of magnetite. Geochim Cosmochim Acta 69: 5639–5646

Song WC, Shao DD, Songsheng LU, Wang XK (2014) Simultaneous removal of uranium and humic acid by cyclodextrin modified graphene oxide nanosheets. SCIENCE CHINA Chem 57:1291–1299

Soudek P, Petrova S, Benesova D, Kotyza J, Vagner M, Vankova R, Vanek T (2010) Study of soil-plant transfer of Ra-226 under greenhouse conditions. J Environ Radioact 101:446–450

Sun Y, Ding C, Cheng W, Wang X (2014) Simultaneous adsorption and reduction of U(VI) on reduced graphene oxide-supported nanoscale zerovalent iron. J Hazard Mater 280:399–408

Tan WF, Wang YC, Mumford K, Li JX, Xu XM, Ding L (2018) Performances of purified indigenous Leifsonia sp. and its mechanism in the removal of Cr(VI) under shaking condition. Int J Environ Sci Technol

Wang JS, Hu XJ, Liu YG, Xie SB, Bao ZL (2010) Biosorption of uranium (VI) by immobilized Aspergillus fumigatus beads. J Environ Radioact 101:504–508

Wang T, Zheng X, Wang X, Lu X, Shen Y (2017) Different biosorption mechanisms of Uranium(VI) by live and heat-killed Saccharomyces cerevisiae under environmentally relevant conditions. J Environ Radioact 167:92–99

Wang et al (2019) Ultra-thin iron phosphate nanosheets for high efficient U(VI) adsorption. J Hazard Mater 371:83–93

Xie Y, Dong H, Zeng G, Tang L, Jiang Z, Zhang C, Deng J, Zhang L, Zhang Y (2017) The interactions between nanoscale zero-valent iron and microbes in the subsurface environment: A review. J Hazard Mater 321:390–407

Yousef LA, Morsy AMA, Hagag MS (2019) Uranium ions adsorption from acid leach liquor using acid cured phosphate rock: kinetic, equilibrium, and thermodynamic studies. Sep Sci Technol 1–10

Zhang Z, Bin et al (2018a) Ordered mesoporous polymer–carbon composites containing amidoxime groups for uranium removal from aqueous solutions. Chem Eng J 341:208–217

Zhang Z, Xin LH, Song W, Ma W, Hu W, Chen T, Liu L (2018b) Accumulation of U(VI) on the Pantoea sp TW18 isolated from radionuclide-contaminated soils. J Environ Radioact 192:219–226

Zhao D, Wang X, Yang S, Guo Z, Sheng G (2012) Impact of water quality parameters on the sorption of U(VI) onto hematite. J Environ Radioact 103:20–29

Zheng XY, Shen YH, Wang XY, Wang TS (2018) Effect of pH on uranium(VI) biosorption and biomineralization by Saccharomyces cerevisiae. Chemosphere 203:109–116